A high-resolution spectral analysis of three carbon-enhanced metal-poor stars⋆

Aruna Goswami[1], Wako Aoki[2], Timothy C. Beers[3], Norbert Christlieb[4,5], John E. Norris[6], Sean G. Ryan[7], Stelios Tsangarides[8]

[1] *Indian Institute of Astrophysics, Koramangala, Bangalore 560034, India; aruna@iiap.res.in*
[2] *National Astronomical Observatory, Mitaka, Tokyo, 181-8588 Japan; aoki.wako@nao.ac.jp*
[3] *Department of Physics and Astronomy, CSCE: Center for the Study of Cosmic Evolution, and JINA: Joint Institute for Nuclear Astrophysics, Michigan State University, East Lansing, MI 48824-1116 USA; beers@pa.msu.edu*
[4] *Hamburger Sternwarte, University of Hamburg, D-21029, Hamburg, Germany*
[5] *Department of Astronomy and Space Physics, Uppsala University, Box 515, SE-75120 Uppsala, Sweden; norbert@astro.uu.se*
[6] *Research School of Astronomy and Astrophysics, Australian National University, Canberra, ACT2611; jen@mso.anu.edu.au*
[7] *Centre for Astrophysics Research, STRI, University of Hertfordshire, College Lane, Hatfield, AL10 9AB, United Kingdom s.g.ryan@herts.ac.uk*
[8] *Department of Physics and Astronomy, Open University, Walton Hall, Milton Keynes, MK7 6AA, England, UK; s.tsangarides@open.ac.uk*

Accepted : Received : in original form :

ABSTRACT

We present results of an analysis of high-resolution spectra ($R \sim 50\,000$), obtained with the Subaru Telescope High Dispersion Spectrograph, of two Carbon-Enhanced Metal-Poor (CEMP) stars selected from the Hamburg/ESO prism survey, HE 1305+0007 and HE 1152−0355, and of the classical CH star HD 5223. All of these stars have relatively low effective temperatures (4000–4750 K) and high carbon abundances, which results in the presence of very strong molecular carbon bands in their spectra. The stellar atmospheric parameters for these stars indicate that they all have surface gravities consistent with a present location on the red-giant branch, and metallicities of [Fe/H] = −2.0 (HE 1305+0007, HD 5223) and [Fe/H] = −1.3 (HE 1152−0355). In addition to their large enhancements of carbon ([C/Fe] = +1.8, +1.6 and +0.6. respectively), all three stars exhibit strong enhancements of the s-process elements relative to iron.

HE 1305+0007 exhibits a large enhancement of the 3rd-peak s-process element lead, with [Pb/Fe] = +2.37, as well as a high abundance of the r-process element europium, [Eu/Fe] = +1.97. The 2nd-peak s-process elements Ba, La, Ce, Nd, and Sm are found to be more enhanced than the 1st-peak s-process elements Zr, Sr and Y. Thus, HE 1305+0007 joins the growing class of the so-called "Lead Stars", and also the class of objects that exhibit the presence of both r-process and s-process elements, the CEMP-r/s stars. The large enhancement of n-capture elements exhibited by HE 1152−0355 and HD 5223 are more consistent with the abundance patterns generally noticed in CH stars, essentially arising from pure s-process nucleosynthesis. The elemental abundance distributions observed in these stars are discussed in the light of existing theories of CH star formation, as well as the suggested formation scenarios of the CEMP-r/s group.

Key words: stars: CH stars - stars: CEMP-r/s - stars: Lead stars - stars: spectral characteristics - stars: AGB - stars: population II - stars: Abundances - stars: Nucleosynthesis -

1 INTRODUCTION

Over the past few decades, detailed studies of the harvest of metal-poor stars from the HK survey of Beers and col-

⋆ Based on data collected at the Subaru Telescope, which is operated by the National Astronomical Observatory of Japan

leagues (Beers, Preston, & Shectman 1985; Beers, Preston, & Shectman 1992; Beers 1999) and the Hamburg/ESO Survey (HES) of Christlieb and collaborators (Christlieb 2003) have revealed them to possess a wide variety of elemental abundance patterns. Among the at-first surprising results was the large fraction of very metal-poor ([Fe/H] < -2.0) stars with large overabundances of carbon relative to iron. Lucatello et al. (2006) estimates the fraction of carbon-enhanced metal-poor (CEMP) stars, defined as having [C/Fe] $> +1.0$, to be on the order of 20% to 25% of very metal-poor stars, once the likely dilution of carbon within their atmospheres is taken into account. Subsequent high-resolution spectroscopic studies of a number of CEMP stars (Norris et al. 1997a 1997b, 2002; Bonifacio et al. 1998; Hill et al. 2000; Aoki et al. 2002; Aoki et al. 2006) has revealed that the CEMP stars can be further subdivided into several classes. According to the suggested taxonomy of Beers & Christlieb (2005), these include: (a) the CEMP-r stars, which exhibit the presence of strong enhancements of r-process elements, (b) the CEMP-s stars, which exhibit the presence of strongly enhanced s-process elements, (c) the CEMP-r/s stars, which apparently have contributions from both of these neutron-capture sources, and (d) the CEMP-no stars, which exhibit no enhancements of neutron-capture elements. Numerous questions remain as to the nucleosynthetic histories and astrophysical sites associated with the production of these classes of carbon-enhanced metal-poor stars. It already seems clear that a single mechanism for the production of the enhanced carbon in these stars would be unlikely to lead to such a diversity of heavy-element abundance patterns.

In order to obtain insight into the possible origins of the CEMP stars, and to place additional constraints on the nucleosynthesis of s-process and r-process elements at low metallicity, it is thus necessary to conduct high-resolution observations of as many types of the CEMP stars as possible. As carbon plays a central role in the nucleosynthesis reactions that drive the post main-sequence evolution of stars, one might also obtain clues into the evolutionary processes by studying the range of carbon abundances and carbon isotope ratios exhibited by CEMP stars.

Christlieb et al. (2001) selected a large sample of carbon-enhanced stars from the HES on the basis of the presence of molecular (e.g, CH, CN, and C_2) bands on the original prism plates, without placing any additional selection on their metallicities. Several teams have been obtaining low- to medium-resolution spectroscopic follow-up of these stars in order to investigate their nature in more detail. Marsteller et al. (in preparation) will report on medium-resolution spectroscopy of over 350 stars from the Christlieb et al. (2001) sample. Goswami (2005) reported spectral classifications for 91 of the Christlieb et al. (2001) stars based on low-resolution spectroscopy ($R = \lambda/\delta\lambda \sim 1330$). In this study some 30% of the sample were shown to be likely CEMP stars. We have undertaken a high-resolution study of these CEMP candidates (with additional targets from Goswami 2006, in preparation) in order to obtain confirmation of their identification with this class, as well as to carry out a comprehensive study of their heavy-element abundance distributions.

This paper reports the first results of our high-resolution spectroscopic campaign, and discusses two candidate CEMP stars from the Goswami (2005, 2006 in preparation) study, HE 1305+0007 and HE 1152−0355. First abundance results for a number of heavy elements in the classical CH star HD 5223 are also presented.

In section 2 we present details of the observations that have been conducted, and describe the low-resolution spectra of our program stars. Section 3 presents $BVRIJHK$ photometry of these stars, and discusses our estimates of their effective temperatures based on this information. The procedures we have adopted for estimation of the stellar atmospheric parameters are discussed in section 4. The elemental abundance results are presented in section 5. Results and discussions of our present study, and consideration of existing theories for the nucleosynthesis history of CEMP-s and CEMP-r/s stars are presented in section 6. Section 7 provides some conclusions.

2 OBSERVATION, DATA REDUCTION, AND RADIAL VELOCITIES

The low-resolution spectra of our program HES stars were obtained with the 2m Himalayan Chandra Telescope (HCT) at the Indian Astronomical Observatory (IAO), Mt. Saraswati, Digpa-ratsa Ri, Hanle, India during January 2005. The spectra of two classical CH stars, HD 5223 and HD 209621, were also obtained with the same telescope. These spectra cover a wavelength range from about 3800 Å to 6800 Å, with a spectral resolving power $R = \lambda/\delta\lambda \sim 1330$. For each star two spectra were taken, each of 15 minutes duration; the spectra were then combined to increase the final signal-to-noise ratio. Observations of a Th-Ar hollow cathode lamp taken immediately before and after the stellar exposures provided the wavelength calibration. Standard spectroscopic reductions (e.g., flat fields, bias subtraction, extraction, and wavelength calibration) were carried out using the IRAF† spectroscopic reduction package.

High-resolution spectroscopic observations of our program stars were carried out with the High Dispersion Spectrograph (HDS) of the 8.2m Subaru Telescope (Noguchi et al. 2002) on 25 May, 2003. Each object spectrum was taken with a 10 minute exposure having a resolving power of $R \sim 50\,000$. The observed bandpass ran from about 4020 Å to 6775 Å, with a gap of about 75 Å, from 5335 Å to 5410 Å, due to the physical spacing of the CCD detectors. These data were also reduced, in the standard fashion, using IRAF.

2.1 Description of the spectra

Figure 1 shows the low-resolution spectra of the two HES stars in the wavelength region 3850 Å to 5000 Å. The spectra of two well-known CH stars HD 5223 and HD 209621, obtained at the same resolving power, are also plotted for comparison. Following Goswami (2005), we note that the two HES stars are potential CEMP (CH) candidate stars. The G band of CH is noticeably strong and appears to be almost of equal strength in all the spectra. The secondary

† IRAF is distributed by the National Optical Astronomical Observatories, which is operated by the Association for Universities for Research in Astronomy, Inc., under contract to the National Science Foundation

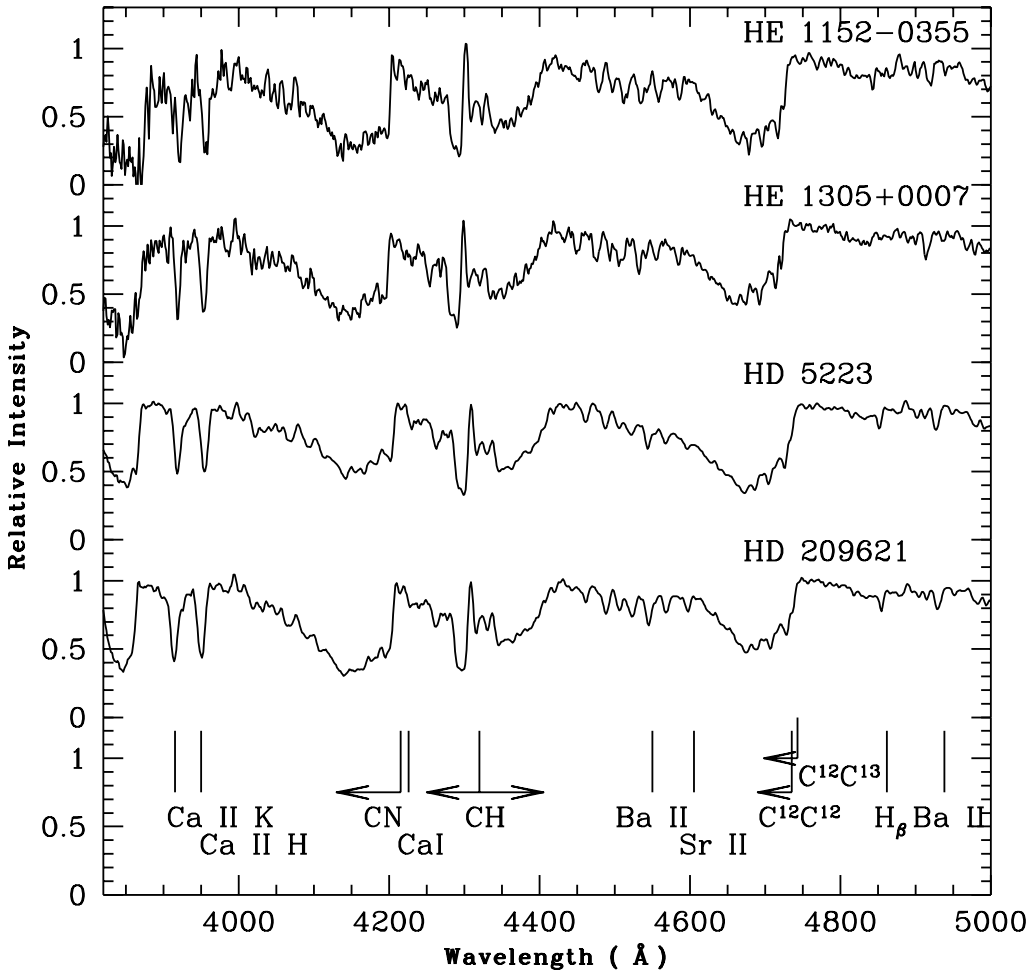

Figure 1. A comparison of the low-resolution spectra of HE 1305+0007 and HE 1152−0355 in the wavelength region 3850 Å to 5000 Å. The spectra of the well-known CH stars HD 5223 and HD 209621 are also plotted for comparison. Prominent atomic and molecular features are indicated.

P-branch head around 4342 Å is distinctly seen in the HES stellar spectra, as well as in HD 5223 and HD 209621. The Ca I feature at 4226 Å is weakly noticed in the two HES stellar spectra. Narrow atomic lines are blended with contributions from molecular bands. As in the case of the two HD stars, Hβ and Ba II at 4554 Å are two clearly noticable features in the HES stellar spectra.

The high-resolution spectra of HE 1305+0007, HE 1152−0355, and HD 5223 are typical of the complex combination of molecular and atomic absorption features in their cool atmospheres. The optical spectra of the stars are characterized by very closely-spaced molecular absorption lines of CH, CN and the Swan system of C_2. The continuum is obscured over essentially the entire wavelength region, and the atomic absorption lines are overwhelmed by the molecular transitions. Measurements of equivalent widths are therefore not free from uncertainties, even in the case of relatively clean lines. Nonetheless, we have identified a number of atomic features on the spectra and measured their equivalent widths, which are used in the present work to derive the elemental abundances using a model-atmosphere analysis.

We have also searched for Li in the high resolution spectra of our three program stars. A wide spread of Li abundances is known to exist among CEMP stars (e.g., Norris, Ryan & Beers 1997a). Although in giants Li is not expected to currently exist on their stellar surfaces due to its likely destruction from internal-mixing processes, it is still worthwhile to search for its presence. If detected, a measure of Li abundance could help understand the formation mechanisms of these objects. Hill et al (2000) have derived a Li abundance for CS 22948-027, (a star very similar to HE 1305+0007) of logϵ(Li) = +0.3, a value much lower than the primordial Li abundance. This is an indication of some internal mixing affecting the surface abundances. Unfortunately, this feature could not be detected in the spectra of our stars.

2.2 Radial velocities

The radial velocities of our program stars were measured using several unblended lines. Estimated heliocentric radial velicities $v_{\rm r}$ of the program stars are shown in Table 1. No previous estimates of radial velocities for HE 1305+0007 and HE 1152−0355 are available in the literature. It is thus presently not known whether these two stars are radial velocity variables. HD 5223, on the other hand, is known to be a radial velocity variable; McClure & Woodsworth (1990) studied its radial velocity variations in detail and reported that $v_{\rm r}$ of HD 5223 ranges from −230 to −250 km s^{-1}. The SIMBAD database lists a mean radial velocity of $v_{\rm r} = -232$ km s^{-1} for this star.

3 PHOTOMETRY

Optical broadband $BVRI$ photometry has been obtained for our program stars (Beers et al. 2006). These data are reported, along with near-IR JHK photometry from 2MASS (Skrutskie et al. 2006), in Table 2. Estimates of the line-of-sight reddening values, $E(B-V)$, for the HES stars listed in Table 2 are obtained from the Schlegel, Finkbeiner, & Davis (1998) dust maps. The reddening estimate for CS 22948-027 is $E(B-V) = 0.00$, as obtained from the Burstein and Heiles (1982) maps, and $E(B-V) = 0.04$ in the case of HD 5223, as obtained from Sleivyte & Bartkevicius (1990).

3.1 Effective temperatures from photometry

Estimates of the effective temperatures of the two HES stars in our program have been determined using the temperature calibrations derived by Alonso et al. (1996), which relate $T_{\rm eff}$ with various optical and near-IR colours. Alonso et al. estimate an external uncertainty in the temperature calculation using this method of ~ 90 K.

The Alonso calibrations of $B-V$, $V-R$, $V-I$, $R-I$ and $V-K$ require colours in the Johnson system, and the calibrations of the IR colours $J-H$, and $J-K$ in the TCS system (the photometric system at the 1.54 m Carlos Sanchez telescope in Tenerife; Arribas & Martinez-Roger 1987). To obtain the $V-K$ colour in the Johnson system we first transformed the K_s 2MASS magnitude to the TCS system. Then, using eqs (6) and (7) of Alonso et al. (1994), K is transformed to the Johnson system from the TCS system. In order to transform the 2MASS colours $J-H$ and $J-K_S$ onto the TCS system we first transformed the 2MASS colours to CIT colours (Cutri et al. 2003), and then from CIT to the TCS system (Alonso et al. 1994).

Estimation of the $T_{\rm eff}$ from the $T_{\rm eff}$ - $(J-H)$ and $T_{\rm eff}$ - $(V-K)$ relations also involves a metallicity ([Fe/H]) term. We have estimated the $T_{\rm eff}$ of the stars at several metallicities. The estimated temperatures, along with the adopted metallicities, are listed in Table 3.

The broadband $B-V$ colour is often used for the determination of $T_{\rm eff}$, however, the $B-V$ colour of a star with strong molecular carbon absorption features depends not only on $T_{\rm eff}$, but also on the metallicity of the star and on the strength of its molecular carbon absorption features, due to the effect of CH molecular absorption in the B band. For this reason, we have not used the empirical $T_{\rm eff}$ scale for the $B-V$ colour indices. The temperatures listed in Table 3 span a wide range; while $J-K$, $J-H$, and $V-K$ colours provide similar temperatures, the $V-I$ colour predict higher temperatures.

4 STELLAR ATMOSPHERIC PARAMETERS

A selection of Fe I and Fe II lines (Table A), covering a range in excitation potential (0.0-4.0 eV) and equivalent widths (20-160 mÅ), was used in a routine procedure to determine the stellar atmospheric parameters – the effective temperature $T_{\rm eff}$, the surface gravity log g, the microturbulence $V_{\rm t}$, and the metallicity [Fe/H]. For HE 1152−0355, a few stronger lines were also used, as the number of lines falling in the above range of equivalent widths is very small. Nineteen Fe I lines in HE 1305+0007, eighteen Fe I lines in HE 1152−0355, and twenty-four Fe I lines (and four Fe II lines) in HD 5223 were found to be useful for our analysis. In Table B, we present the measured equivalent widths for other elements. In this Table, the star HE 1152-0355 is not included, due to the severe contamination by molecular absorption features in this object, which prevented reasonable fits of gaussian line profiles to be obtained. This star is also the coolest among the three. Throughout our analysis we have assumed that local thermodynamic equilibrium conditions apply. Model atmospheres were selected from the Kurucz grid of model atmospheres with no convective overshooting, and from those that are newly computed models with better opacities and abundances. These models are available at `http://cfaku5.cfa.harvard.edu/`, labelled with the suffix "odfnew". For our analysis, the excitation potentials and oscillator strengths of the lines were taken from various sources, including the Vienna Atomic Line Database (`http://ams.astro.univie.ac.at/vald/`) and also the Kurucz atomic line list (`http://cfa-www.harvard.edu/-amdata/ampdata/kurucz23/sekur.html`), Fuhr, Martin, & Wiese (1988), Martin, Fuhr, & Wiese (1988), and Lambert et al. (1996). The gf values for some elements were also taken from a compilation assembled by R.E. Luck (private communication); these are based, when possible, on experimental determinations of high quality. We have employed the latest (2002) version of MOOG, an LTE stellar line-analysis program (Sneden 1973).

The microturbulent velocity is generally estimated at a given effective temperature by demanding that there should be no dependence of the derived Fe I abundance upon the equivalent widths of Fe I lines. However, in the present case, the number of usable lines is small. The wavelength regions around the lines at 4863, 4892, 5753 and 5806 Å that are used in our analysis are significantly affected by C_2 and CN molecular features. It is therefore possible that the equivalent widths of these lines are overestimated due to contamination from molecular features. This in turn would affect the determination of microturbulent velocity. Taking this into consideration, and following the discussions of Vanture (1992) and McWilliam et al. (1995) ($V_{\rm t}$ in cool giants with $\log g \leq 2.0$ are in general ≥ 2 km s^{-1}), we have adopted a value of $V_{\rm t} = 2$ km s^{-1} for both of the HES stars and for HD 5223.

Estimates of effective temperatures were then obtained by the method of excitation balance, forcing the slope of the

Table 1: Heliocentric Radial velicities v_r of the program stars

Stars	v_r km s^{-1} our estimation	HJD	v_r km s^{-1} from literature
HE 1305+0007	+217.8 ± 1.5	2452784.95121	—
HE 1152−0355	+431.3 ± 1.5	2452784.83629	—
HD 5223	−244.9 ± 1.5	2453544.12049	−232

Table 2: Photometric parameters for program and comparison stars

Stars	RA(2000)	Dec(2000)	V	$B-V$	$V-R$	$V-I$	$E(B-V)$	J	H	K_s
HE 1305+0007	13 08 03.84	−00 08 47.3	12.22	1.459	0.682	1.152	0.038	10.247	9.753	9.600
HE 1152−0355	11 55 06.10	−04 12 24.0	11.43	2.459	0.816	1.194	0.026	9.339	8.665	8.429
HD 5223	00 54 13.61	+24 04 01.5	8.47	1.43	—	—	0.04	6.372	5.845	5.673
CS 22948-027	21 37 45.80	−39 27 22.0	12.65	1.12	0.5	0.90	0.00	10.979	10.534	10.427

abundances from Fe I lines versus excitation potential to be near zero. The temperature estimates in Table 3 provided a preliminary temperature check for the program stars; model atmospheres corresponding to these temperatures were used initially, and the adopted effective temperatures were then obtained by an iterative process using the method of excitation balance. In Figure 2, we show the iron abundances of two examples, HE 1305+0007 and HD 5223, for individual Fe I and Fe II lines as a function of each line's equivalent width and the lower excitation potential. If we rely on the Fe I excitation equilibrium, with an adopted microturbulance of 2 km s^{-1}, we estimate the effective temperatures for HE 1305+0007 and HE 1152−0355 to be 4750 K and 4000 K, respectively. For HD 5223, the estimated $T_{\rm eff}$ is 4500 K. Using the Fe I/Fe II ionisation equilibrium, the surface gravities of HE 1305+0007, HE 1152−0355 and HD 5223 are obtained to be log g = 2.0, 1.0 and 1.0, respectively. The derived metallicities are [Fe/H] = −2.0, −1.3 and −2.0, respectively (Table 4).

Vanture (1992) reported a higher metallicity, [Fe/H] = −0.9, for HD 5223, even though his estimates of $T_{\rm eff} \sim 4550$ K and $\log g \sim 1.3$ are very similar to those we have adopted. To verify our estimations, we have determined the atmospheric parameters for the star CS 22948-027 (a star very similar to HE 1305+0007, see section 6) and compared with those given by other authors. We obtained similar results to those reported by Barbuy et al. (2005). They estimated $T_{\rm eff}$ = 4800K, $\log g$ = 1.8, $V_{\rm t}$ = 1.5 and [Fe/H] = −2.46, very close to our present estimates (Table 4).

5 ABUNDANCE ANALYSIS

There are numerous features, from a variety of elements, identified in our program star spectra (Table B). However, throughout the spectral range the line blending is so severe that for most elements a standard abundance analysis procedure based on the equivalent widths could not be applied, and the abundances must be derived from spectrum-synthesis calculations. A fit of the synthetic spectrum in the wavelength region 5170 to 5190 Å, obtained using the atmospheric parameters listed in Table 4, is illustrated in Figure 3. This region is relatively free from contamination by molecular features. The method of spectrum synthesis is also applied to lines that are affected by hyperfine splitting. For the spectrum synthesis of lines, we find that a projected velocity $v\sin i$ of 5.0 ± 2 km s^{-1} matches the widths of the observed features with those of the synthetic spectra. This value represents the sum of macroscopic broadening, and does not necessarily indicate significant rotation of the star. In Table 5 we present abundances derived from spectrum-synthesis calculations. In this Table we have listed not only the abundance log ϵ(X), and [X/H], but also [X/Fe]. In computing the quantity [X/Fe], we have used the Fe I-based abundance for elemental abundances derived from neutral lines and the Fe II-based abundance for elemental abundances derived from ionized lines. Local thermodynamic equilibrium was assumed for all of the spectrum-synthesis calculations. We have used the latest version of MOOG for spectrum synthesis. The line lists for each region that is synthesized are taken from the Kurucz atomic line list (`http://cfa-www.harvard.edu/amdata/ampdata/-kurucz23/sekur.html`) and from the Vienna Atomic Line Database (`http://ams.astro.univie.ac.at/vald/`). Reference solar abundances for the various elemental species were adopted from Asplund, Grevesse & Sauval (2005). The log gf values for atomic lines were adopted from Fuhr et al. (1988) and Martin et al. (1988), whenever available, and also from a compilation of gf values by R. E. Luck (private communication). The heavy neutron-capture elements lines and corresponding log gf values given by Sneden et al. (1996) and Lawler et al. (2001) were also consulted.

For HE 1305+0007, we have determined the abundances of C, Na, Mg, Ca, Sc, Ti, Mn, Ni, and among the heavy elements, Sr, Y, Zr, Ba, La, Ce, Pr, Nd, Sm, Eu, and Pb. Abundances of several heavy s-process elements, in addition to the carbon abundance, are also determined for HE 1152−0355. For HD 5223 we could determine the abundances of C, Na, Mg, Ca, Ti, Ni, Sr, Y, Zr, Ba, La, Ce, Nd, Sm, and Pb. Details of the behaviour of the elemental abundance patterns for our program stars are discussed below.

5.1 Carbon

The carbon (C) abundance is derived from spectral synthesis of the C_2 Swan 0-1 band around 5635 Å. A synthetic spectrum, derived using a carbon abundance of log ϵ(C) =

Table 3: Estimated effective temperatures ($T_{\rm eff}$) from semi-empirical relations

Star Names	$T_{\rm eff}$ $(J-K)$	$T_{\rm eff}$ $(J-H)$	$T_{\rm eff}$ $(V-K)$	$T_{\rm eff}$ $(V-R)$	$T_{\rm eff}$ $(V-I)$
HE 1305+0007	4636	4697.2 (−1.5)	4497.8 (−1.5)	4949.9 (−1.5)	5043.4
		4714.3 (−2.0)	4376.2 (−2.0)	4931.2 (−2.0)	—
HE 1152−0355	3756	3985.9 (−1.0)	4133.4 (−1.0)	4529.8 (−1.0)	4963.2
		4002.3 (−1.5)	4083.8 (−1.5)	4451.8 (−1.5)	—
HD 5223	4360	4539.0 (−1.0)	4298.5 (−1.0)	—	—
		4555.9 (−1.5)	4253.9 (−1.5)	—	—
		4572.9 (−2.0)	4213.8 (−2.0)	—	—
CS 22948−027	4892	4903.8 (−1.0)	4840.5 (−1.0)	5784.8 (−1.0)	5629.8
		4920.7 (−1.5)	4815.8 (−1.5)	5758.4 (−1.5)	—
		4937.7 (−2.0)	4796.1 (−2.0)	5755.1 (−2.0)	—

The numbers inside the parentheses indicate the adopted metallicities [Fe/H]

8.2 ± 0.3, combined with the appropriate model atmosphere, shows a good match to the depth of the observed spectrum of HE 1305+0007. Relative to the solar photospheric C abundance, C is strongly enhanced in HE 1305+0007 ([C/Fe] = +1.84). A similar procedure returns a C abundance of log ϵ(C) = 7.7 ± 0.1 for HE 1152−0355 ([C/Fe] = +0.58), and log ϵ(C) = 7.9 ± 0.2 for HD 5223 ([C/Fe] = +1.57).

Carbon abundances derived from the spectrum synthesis of the CH G-band are not considered. This feature is severely saturated in our objects, is quite insensitive to the carbon abundance, and hence likely to return uncertain values. Spectrum synthesis of the C_2 Swan 0-1 band around 5635 Å is, however, found to provide the most reasonable estimates. Spectrum-synthesis fits for HE 1305+0007, HE 1152−0355, and HD 5223 are shown in Figure 4.

5.2 The odd-Z elements Na and Al

The sodium (Na) abundance in HE 1305+0007 is calculated from the resonance doublet – the Na I D lines at 5890 Å and 5896 Å. These resonance lines are sensitive to non-LTE effects (Baumüller & Gehren 1997; Baumüller et al. 1998; Cayrel et al. 2004). The derived abundance from an LTE analysis displays an overabundance with respect to Fe of [Na/Fe] = +0.26, based on the Na I D_2 line, and an overabundance [Na/Fe] = +0.43, based on the Na I D_1 line. This abundance may be therefore slightly overestimated (the non-LTE case is not considered here). As a result of the severe line asymmetry of the Na I resonance doublet, due to molecular contamination, we could not estimate the Na abundance in the star HE 1152−0355. In CS 22948-027, an upper limit of the Na abundance was estimated to be [Na/Fe] < +0.57 by Barbuy et al. (2005). This value is slightly higher than what we have obtained for HE 1305+0007, a star very similar to this object. For HD 5223, the Na abundance is derived using the Na I D lines, and found to be [Na/Fe] = +0.46. While Na exhibits a mild overabundance in HE 1305+0007 and CS 22948-027, it is interesting to note that the excess of Na is quite significant in CS 29497-034, a star which is otherwise very similar to both HE 1305+0007 and CS 22948-027. This star also has the lowest metallicity amongst these three.

The aluminum (Al) lines are severely blended in the spectra of our program stars, and could not be used for abundance determination. The Al line at 3961.5 Å, which is generally used for Al abundance determination in extremely metal-poor stars, lies outside the wavelength range of our spectra.

5.3 The α-elements Mg, Si, Ca, and Ti

Several lines due to α-elements were identified in the spectra of the two HES stars. However, in order to avoid contamination problems from the strong molecular carbon features, we have selected the cleanest line of each element, and derived the abundance from spectrum-synthesis calculations. Hence, in many cases, the abundance is derived from a single-line spectrum-synthesis calculation.

The Mg abundance in HE 1305+0007 is derived from the synthesis of the Mg I line at 5172.68 Å. The predicted line profile with our adopted Mg abundance (log ϵ(Mg) = 5.75) fits the observed line profile in HE 1305+0007 quite well. Magnesium is found to exhibit the usual halo-star overabundance, [Mg/Fe] $\sim$ +0.25. In HE 1305+0007 and HD 5223, the Mg abundances are practically as expected for a halo star with [Fe/H] = −2.0; i.e., showing the classical enhancement of the α-elements (see Goswami & Prantzos 2000, Figure 7). Spectrum synthesis of this line in HE 1152-0355, however, returns an almost solar value of [Mg/Fe] = −0.01. The calcium (Ca) abundance is derived from spectrum synthesis of the Ca I line at 6102.7 Å. Calcium also exhibits a normal halo overabundance of [Ca/Fe] = +0.13 and +0.1 in HE 1305+0007 and HD 5223, respectively. The titanium (Ti) abundance derived from the synthesis of the Ti II line at 4805.085 Å shows a marked overabundance of [Ti/Fe]$\sim$+0.8 in HE 1305+0007. For HD 5223, Ti is overabundant with respect to iron by +0.5 dex.

Due to the presence of severe line blending, the α-element abundances, with the exception of Ti, could not be derived in the star HE 1152−0355. As in the case of HE 1305+0007, the Ti abundance in HE 1152−0355 is also derived from a spectrum synthesis of the Ti II line at 4805.085 Å; we obtain [Ti/Fe] $\sim$ +0.5 for HE 1152-0355.

5.4 The iron-peak elements Mn and Ni

For HE 1305+0007, a spectrum synthesis of the Mn I line at 5432.56 Å returned an abundance estimate of log ϵ(Mn) = 3.5; [Mn/Fe] is found to be almost solar in this star, with [Mn/Fe] = +0.14. A Mn abundance could not be determined for HE 1152−0355 and HD 5223.

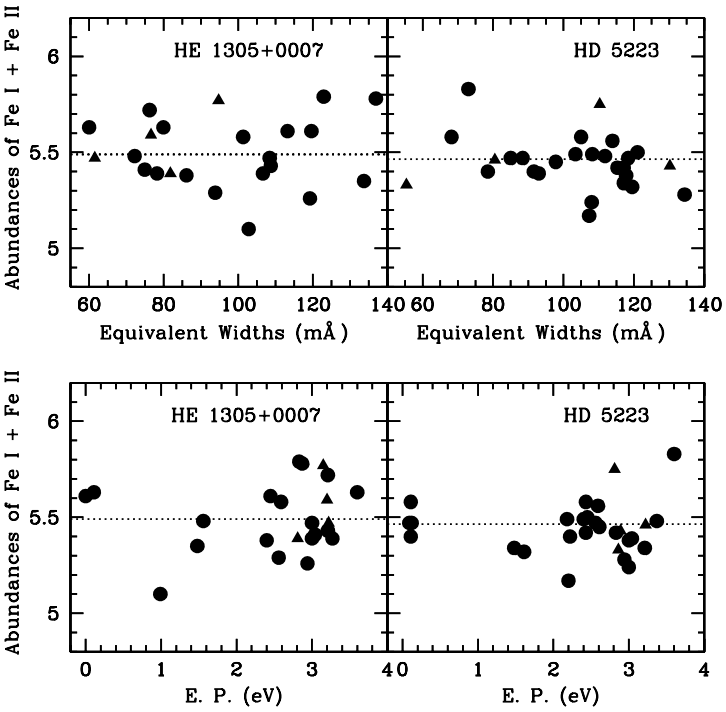

Figure 2. The iron abundance of HE 1305+0007 (left panels) and HD 5223 (right panels) are shown for individual Fe I and Fe II lines as a function of the line's equivalent width (upper panels) and the lower excitation potential (lower panels). The solid circles indicate Fe I lines and the solid triangles indicate Fe II lines.

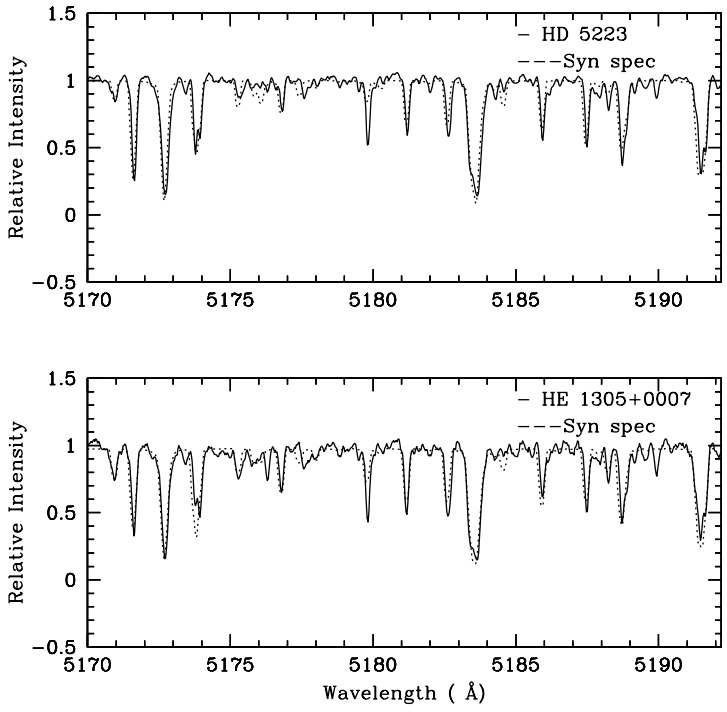

Figure 3. A fit of the synthetic spectrum (dotted curve) compared with the observed spectrum (solid curve) of HD 5223 (upper panel) and HE 1305+0007 (lower panel) in the wavelength region 5170 to 5190 Å. The synthetic spectra are obtained using a model atmosphere corresponding to the adopted parameters listed in Table 4.

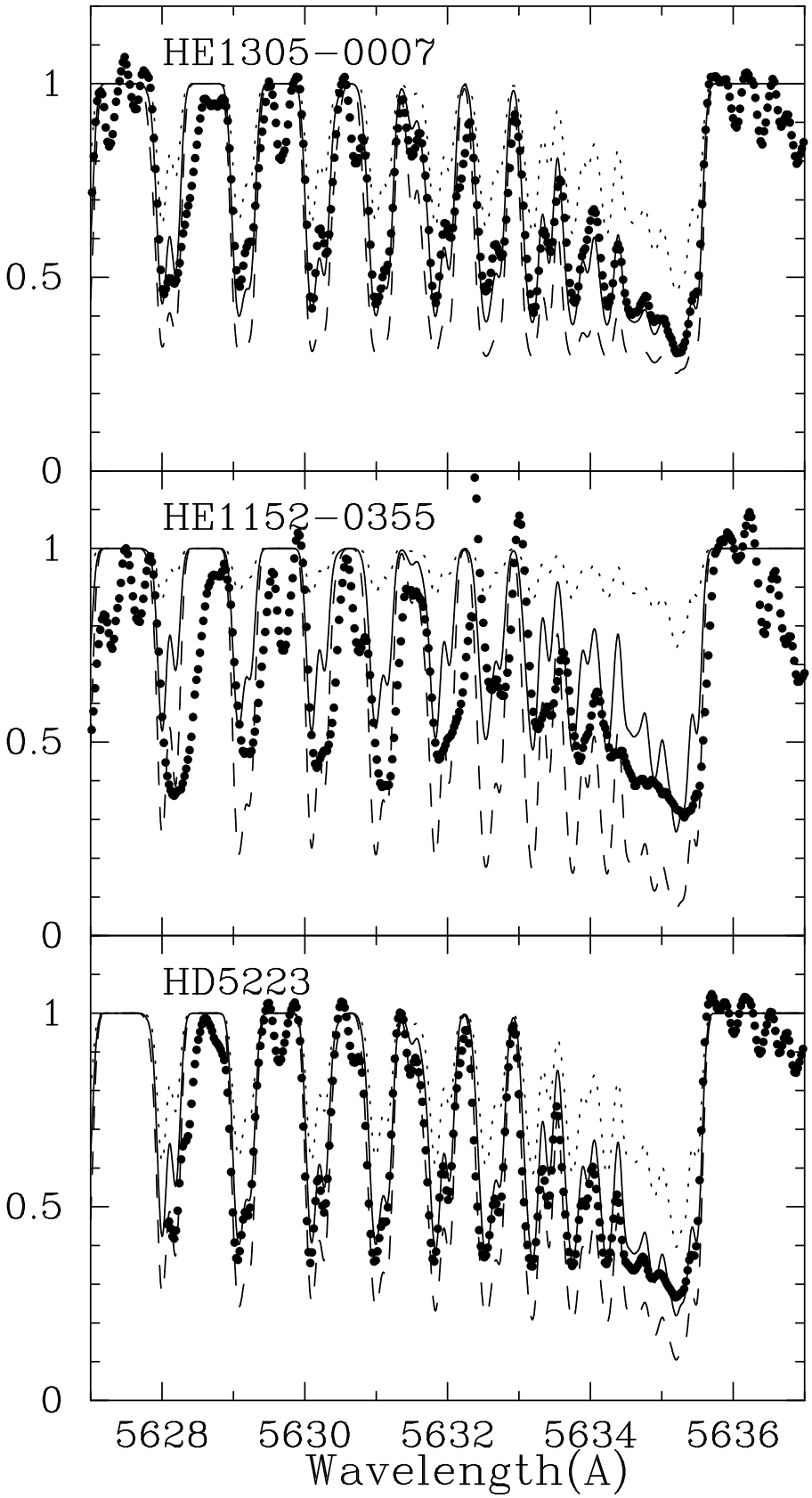

Figure 4. A comparison of the fits of the synthetic spectra for log ϵ(C) = 8.2 ± 0.3 (top), 7.7 ± 0.1 (middle) and 7.9 ± 0.2 (bottom) (represented by solid line, dash and dotted curve, respectively) with the observed spectrum of HE 1305+0007, HE 1152−0355, and HD 5223, respectively (shown by solid circles) in the wavelength region around 5635 Å of the C_2 Swan 0-1 bands. Carbon abundances of log ϵ(C) = 8.2, 7.7, and 7.9 provide the best fit (solid line) of the synthetic spectra with the observed spectra of HE 1305+0007, HE 1152−0355, and HD 5223, respectively.

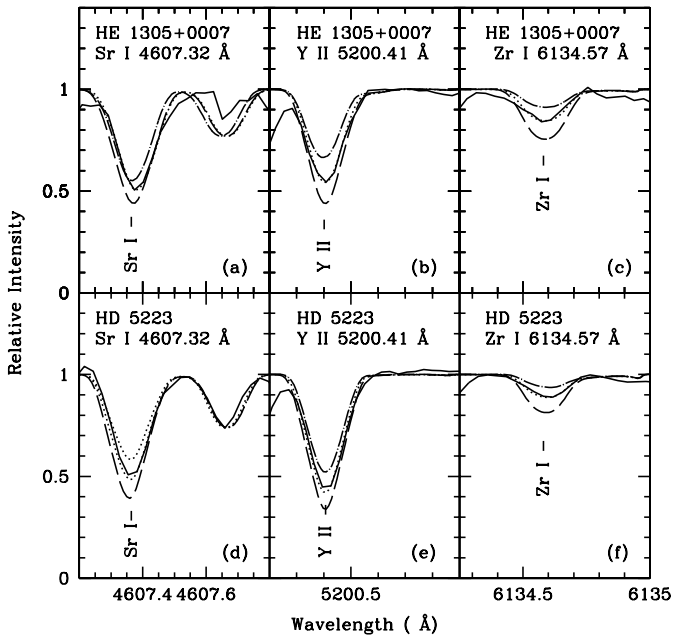

Figure 5. Spectral-synthesis fits of absorption lines arising from the light s-process elements Sr, Y, and Zr, obtained with the elemental abundances listed in Table 5. The dotted lines indicate the synthesized spectra and the solid lines indicate the observed line profiles. Two alternative synthetic spectra for Δ[X/Fe] = +0.3 (long dash) and Δ[X/Fe] = −0.3 (dot-dash) are shown to demonstrate the sensitivity of the line strength to the abundances.

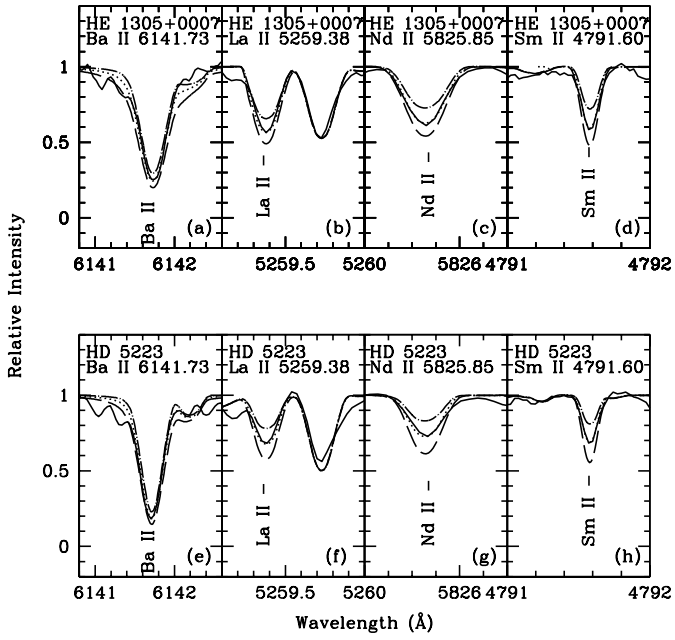

Figure 6. Spectral-synthesis fits of absorption lines arising from the heavy s-process elements Ba, La, Nd, and Sm, obtained with the respective elemental abundances listed in Table 5. The dotted lines indicate the synthesised spectra and the solid lines indicate the observed line profiles. Two alternative synthetic spectra for Δ[X/Fe] = +0.3 (long dash) and Δ[X/Fe] = −0.3 (dot-dash) are shown to demonstrate the sensitivity of the line strength to the abundances.

Nickel abundances in our study are derived from a spectrum synthesis of the Ni I line at 6314.66 Å. Nickel exhibits a mild underabundance of [Ni/Fe] = −0.25 in HE 1305+0007, and an underabundance of [Ni/Fe] = −0.47 in HD 5223.

For very metal-poor stars, a general decrease of the ratios of Mn and Cr, relative to Fe, was initially found by McWilliam et al. (1995) and Ryan, Norris, & Beers (1996). The observational scatter in these trends was lowered considerably by the more recent higher-quality data of Cayrel et al. (2004). Our measured abundances for both of these species fit well with the Cayrel et al. trends.

5.5 The light s-process elements Sr, Y, and Zr

Abundances of the light s-process elements strontium (Sr), yttrium (Y), and zirconium (Zr) are also determined from spectrum-synthesis calculations. The Sr abundance is derived from spectrum synthesis of the Sr I line at 4607.327 Å, the Y abundance from the Y II line at 5200.41 Å, and the Zr abundance is derived from the Zr I line at 6134.57 Å. Examples are shown in Figure 5. In HE 1305+0007, Sr, Y, and Zr exhibit overabundances of [Sr/Fe] = +0.86, [Y/Fe] = +0.73, and [Zr/Fe] = +2.09, respectively. In HE 1152−0355, Y and Zr are found to be almost solar. A spectrum synthesis calculation of Sr line could not be done being highly blended . In HD 5223, Sr, Y, and Zr exhibit overabundances of [Sr/Fe] = +1.39, [Y/Fe] = +0.63, and [Zr/Fe] = +1.57, respectively.

5.6 The heavy n-capture elements: Ba, La, Ce, Pr, Nd, Sm, Eu, Pb

As in the case of the other elements, the abundances of barium (Ba), lanthanum (La), cerium (Ce), neodymium (Nd), and samarium (Sm) are also determined using spectrum-synthesis calculations (examples are shown in Figure 6 and Figure 7). The derived abundances for these elements are found to be overabundant with respect to Fe in all three of our program stars. In the case of HE 1305+0007, abundances of a few more heavy elements, such as Pr, Eu, and Pb, are also determined (Figure 8).

We have not used any hyperfine-splitting corrections for Ce, Nd, and Y lines, since they are very weak, and the abundances are not expected to be affected by hyperfine splitting (McWilliam et al. 1995).

In the case of Ba the hyperfine-splitting (HFS) corrections depend on the r/s fraction assumed to have contributed to the enrichment of the star. This element has both odd and even isotopes. The odd isotopes are mainly produced by the r-process and have a broad HFS, while the even isotopes are mainly produced by the s-process, and exhibit no HFS. However, it was shown by Sneden et al. (1996) that this issue is important for the Ba lines at 4554 Å and 4934 Å, and unimportant for the three other Ba lines at 5854, 6142, and 6497 Å, which are generally used for abundance determination. We have used the red Ba II line at 6141.73 Å for the abundance determination in our stars. The HFS splitting of this line is ∼1/5 of the Ba 4554 Å splitting and ∼1/3 of the thermal line width, and hence we have neglected HFS corrections. Ba is found to exhibit a marked overabundance of [Ba/Fe] = +2.32 in HE 1305+0007, [Ba/Fe] = +1.58 in HE 1152−0355, and [Ba/Fe] = +1.82 in HD 5223.

Lanthanum (La) abundances are derived from a spectrum-synthesis calculation of the La II line at 5259.38 Å, with atomic data taken from Lawler et al. (2001). Similar to Ba, La also exhibits an overabundance of [La/Fe] = +2.56 in HE 1305+0007, [La/Fe] = +1.57 in HE 1152−0355, and [La/Fe] = +1.76 in HD 5223. Neodymium abundances are derived using the Nd II line at 5825.85 Å. Neodymium is also found to be highly overabundant in HE 1305+0007, with [Nd/Fe] = +2.59, whereas, in HE 1152−0355 this element is only mildly overabundant, with [Nd/Fe] = +0.43. In HD 5223, [Nd/Fe] = +1.54.

Samarium (Sm) abundances are derived from the Sm II line at 4790.60 Å. In HE 1305+0007 , Sm exhibits an overabundance of [Sm/Fe] = +2.60, while in HE 1152−0355 and HD 5223, overabundances of [Sm/Fe] = +0.87 and [Sm/Fe] = +1.68 are found, respectively.

In the spectrum of HE 1305+0007 we could also determine the europium (Eu) abundance. Eu is usually considered to be produced almost solely by the r-process in solar-system material. The main lines of this element that are generally used in abundance analysis are the Eu II lines at 4129.7, 4205.05, 6437.64 and 6645.13 Å. The blue Eu II lines at 4129.7 and 4205.05 Å are severely blended with strong molecular features in this star, and could not be used for abundance analysis. The abundance of Eu in HE 1305+0007 is therefore determined from the red lines at 6437.64 Å and 6645.13 Å, using spectrum-synthesis calculations. Both of the lines return an abundance of log ϵ(Eu) = 0.50, indicating that Eu is highly overabundant in HE 1305+0007 ([Eu/Fe] = +1.97). Illustrations of the spectral synthesis for the Eu lines at 6437.64 and 6645.13 Å are shown in Figure 8.

Abundances of cerium (Ce) and praeseodymium (Pr) are derived from spectrum-synthesis calculations of the Ce II line at 5274.23 Å and the Pr II line at 5259.7 Å, respectively. Both of these elements exhibit large overabundances in HE 1305+0007; [Ce/Fe] = +2.53 and [Pr/Fe] = +2.38, respectively. In HD 5223, [Ce/Fe] = +1.87, hence it is also strongly overabundant.

We have also used spectrum-synthesis calculations to determine the abundances of Pb in HE 1305+0007, using the Pb I line at 4057.8 Å. This line is strongly affected by molecular absorption of CH (as indicated in Figure 8). CH lines are included in our spectrum synthesis calculation of Pb abundance. The best spectrum-synthesis fit with the observed line profile is obtained with a lead abundance of log ϵ(Pb) = 2.38, as shown in Figure 8, an overabundance with respect to iron of [Pb/Fe] = +2.37. This line could not be detected in the spectrum of HE 1152−0355. Spectrum synthesis of this line returns a lead abundance of log ϵ(Pb) = 2.15 in HD 5223, with a corresponding overabundance of [Pb/Fe] = +2.21.

5.7 Error Analysis

Errors in the derived abundances arise mainly from two sources, random errors as well as systematic errors arising from uncertainties in our adopted atmospheric parameters. Errors arising due to uncertainties in line parameters, such as the adopted gf values and equivalent width measurements, are usually random and cause line-to-line scatter in derived abundances for a given species. The random errors

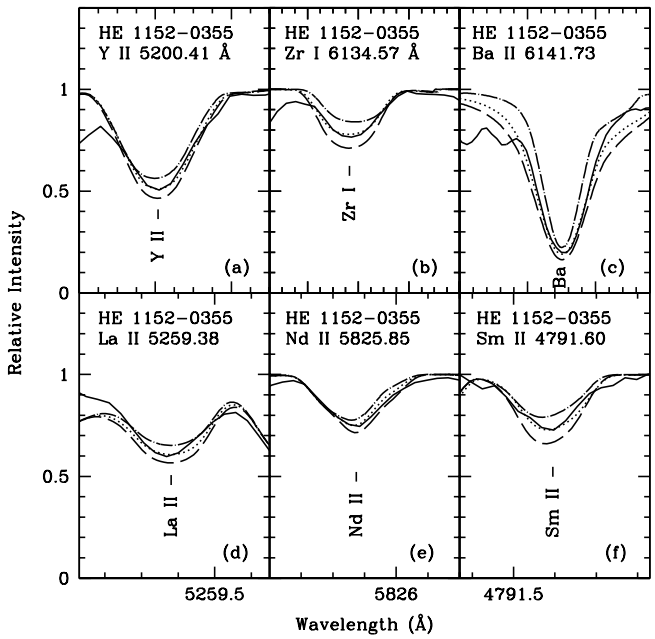

Figure 7. Spectral-synthesis fits of absorption lines arising from the heavy s-process elements Y, Zr, Ba, La, Nd, and Sm, obtained with the respective elemental abundances listed in Table 5. The dotted lines indicate the synthesised spectra and the solid lines indicate the observed line profiles. Two alternative synthetic spectra for Δ[X/Fe] = +0.2 (long dash) and Δ[X/Fe] = −0.2 (dot-dash) are shown to demonstrate the sensitivity of the line strength to the abundances.

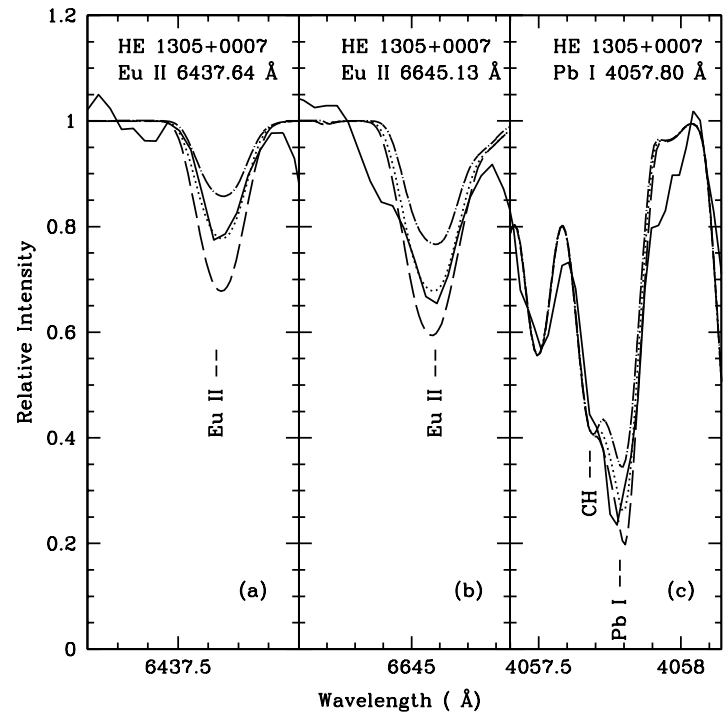

Figure 8. Spectral-synthesis fits of the two Eu II lines at 6437.64 Å and 6645.13 Å, obtained with an europium abundance of log ϵ(Eu) = 0.50. The spectral-synthesis fit of the Pb I line at 4057.80 Å is obtained with log ϵ(Pb) = 2.38. The dotted lines indicate the synthesized spectra and the solid lines indicate the observed line profiles. Two alternative synthetic spectra for Δ[X/Fe] = +0.3 (long dash) and Δ[X/Fe] = −0.3 (dot-dash) are shown to demonstrate the sensitivity of the line strength to abundances.

Table 4: Derived atmospheric parameters

Star Names	$T_{\rm eff}$	$\log g$	$V_{\rm t}$ km s^{-1}	[Fe I/H]	[Fe II/H]
HE 1305+0007	4750	2.0	2.0	−2.03	−1.99
HE 1152−0355	4000	1.0	2.0	−1.27	−1.30
HD 5223	4500	1.0	2.0	−2.06	−2.04
CS 22948-027	4750	1.5	2.0	−2.50	−2.40

Table 5: Chemical compositions

Element	Z	Solar[a]	HE 1305+0007			HE 1152−0355			HD 5223		
		log ϵ	log ϵ	[X/H]	[X/Fe]	log ϵ	[X/H]	[X/Fe]	log ϵ	[X/H]	[X/Fe]
C I	6	8.39	8.20	−0.19	+1.84	7.7	−0.69	+0.58	7.9	−0.49	+1.57
Na I D_2	11	6.17	4.40	−1.77	+0.26	—	—	—	4.57	−1.60	+0.46
Na I D_1	11	6.17	4.57	−1.60	+0.43	—	—	—	4.57	−1.60	+0.46
Mg I	12	7.53	5.75	−1.78	+0.25	6.25	−1.28	−0.01	6.05	−1.48	+0.58
Ca I	20	6.31	4.41	−1.90	+0.13	—	—	—	4.35	−1.96	+0.10
Sc II	21	3.05	1.15	−1.90	+0.09	—	—	—	—	—	—
Ti II	22	4.9	3.70	−1.20	+0.79	4.15	−0.75	+0.52	3.35	−1.55	+0.49
Mn I	25	5.39	3.50	−1.89	+0.14	—	—	—	—	—	—
Fe I	26	7.45	5.42±0.18	−2.03	—	6.18±0.27	−1.27	—	5.39±0.13	−2.06	—
Fe II	26	7.45	5.46±0.17	−1.99	—	6.15±0.24	−1.30	—	5.41±0.18	−2.04	—
Ni I	28	6.23	3.95	−2.28	-0.25	—	—	—	3.70	−2.53	−0.47
Sr I	38	2.92	1.75	−1.17	+0.86	—	—	—	2.25	−0.67	+1.39
Y II	39	2.21	0.95	−1.26	+0.73	1.05	−1.16	+0.14	0.80	−1.41	+0.63
Zr I	40	2.59	2.65	+0.06	+2.09	1.32	−1.27	0.0	2.10	−0.49	+1.57
Ba II	56	2.17	2.50	+0.33	+2.32	2.45	+0.28	+1.58	1.95	−0.22	+1.82
La II	57	1.13	1.70	+0.57	+2.56	1.40	+0.27	+1.57	0.85	−0.28	+1.76
Ce II	58	1.58	2.12	+0.54	+2.53	—	—	—	1.75	−0.17	+1.87
Pr II	59	0.71	1.10	+0.39	+2.38	—	—	—	—	—	—
Nd II	60	1.45	2.05	+0.60	+2.59	0.58	−0.87	+0.43	0.95	−0.50	+1.54
Sm II	62	1.01	1.62	+0.61	+2.60	0.58	−0.43	+0.87	0.65	−0.36	+1.68
Eu II	63	0.52	0.50	−0.02	+1.97	—	—	—	—	—	—
Pb I	82	2.00	2.38	+0.38	+2.37	—	—	—	2.15	+0.15	+2.21*

[a] Asplund, Grevesse & Sauval (2005); * indicates an upper limit

are minimized by employing as many usable lines as possible for a given element. In deriving the Fe abundances we made use of 19, 18, and 24 Fe I lines and 4, 2, and 4 Fe II lines in HE 1305+0007, HE 1152-0355 and HD 5223, respectively. The derived standard deviation σ is defined by $\sigma^2 = [\Sigma(\chi_i - \chi)^2/(N-1)]$, where N is the number of lines used. The values of σ computed from the Fe I lines are ±0.18 dex, ±0.27 dex and ±0.13 dex in HE 1305+0007, HE 1152-0355, and HD 5223, respectively. The corresponding values for these three stars calculated for Fe II lines are ±0.17 dex, ±0.24 dex, and ±0.18 dex, respectively. Errors arising from the random uncertainties are computed when the number of clean lines (N) measured is ≥ 2 for a given element. The computed errors for Fe I and Fe II are listed in Table 5.

Uncertainties in the adopted model atmospheric parameters may also introduce errors in derived abundances. The accuracy of the atmospheric parameters was estimated by computing a set of Fe I lines for pairs of models with (a) the same gravity and microturbulence velocity but different temperatures (b) with the same temperature and gravity but different microturbulent velocities and (c) with the same temperature and microturbulent velocity but different gravities. A comparison of the variations in the computed equivalent widths for the three cases with the accuracy of equivalent width measurements allowed us to estimate the uncertainties in the determination of the atmospheric parameters. The (conservative) uncertainties in the estimated $T_{\rm eff}$ is $\pm 250K$, in surface gravity log g ±0.25 dex, and in microturbulent velocity $V_{\rm t}$ ± 0.25 km s^{-1}. Errors in the abundances arising from the errors in atmospheric parameters are not a simple sum of the errors due to the individual parameters. These parameters interact with one another and a change in one may cause a shift in another. The net effect on the derived mean abundances should be considerably less, because we employ the principle of consistency wherein the lines with a large range of excitation potentials, equivalent widths, and different ionization states should lead us to the same value of abundances.

In Table 6, we take HE 1305+0007 as an example, and derive differential abundances of elements with respect to those obtained from the adopted model ($T_{\rm eff}$ = 4750 K, log g = 2.0, and $V_{\rm t}$ = 2.0 km s^{-1}). These errors are estimated by varying $T_{\rm eff}$ by ± 250 K, log g by 0.25 dex, and $V_{\rm t}$ by 0.25 km s^{-1} in the adopted stellar atmosphere models of HE 1305+0007. Computation of abundance errors for the other two stars yields similar results.

The abundances of all other elements listed in Table 5 are derived by spectrum synthesis calculation. In these cases we have visually estimated the fitting errors. Our estimated fitting errors range between 0.1 dex and 0.3 dex. We adopt these fitting errors as estimates of the random errors associated with the derived elemental abundances. In Figures 4

through 8, we have shown synthetic spectra for the adopted element abundances compared with the synthetic spectra due to two other possible abundances with ±0.2 dex or ±0.3 dex (see figure captions) differences with respect to our adopted abundances.

6 RESULTS AND INTERPRETATIONS

We have reported a high-resolution spectroscopic analysis of the CEMP stars HE 1305+0007 and HE 1152−0355, which belong to the somewhat lesser studied group of objects of cool CEMP stars. A detailed analysis of high-resolution spectroscopy for HD 5223, a well-known classical CH star (used by Goswami 2005, 2006 as a comparison star), has also been reported.

Our analysis confirms that HD 5223 and the two HES stars are all highly carbon-enhanced metal-poor stars. One characteristic feature of CH (CEMP-s) stars is that the heavy 2nd -peak s-process elements, such as Ba, La, Ce, Nd, and Sm, are more enhanced than the lighter 1st-peak s-process elements Sr, Y and Zr. All three of our program stars exhibit this behaviour (Table 5).

Radial-velocity measurements (Table 1) indicate that all three objects are high-velocity stars, and likely to be members of the Galactic halo population. While we have measured a radial velocity of +217.8 km s^{-1} in the case of HE 1305+0007, for HE 1152-0355 we have measured +431.3 km s^{-1}, almost twice as high. Such a high velocity for halo stars is rare but not exceptional; an inspection of high proper motion stars (Carney et al. 1994) reveals three stars, namely G 64−12, G 241−4, and G 233−27 with absolute velocities greater than 400 km s^{-1}. From the high radial velocity of HE 1152-0355, one could speculate that the star could be a runaway from a binary companion that exploded (in the context of Qian and Wasserburg 2003 scenarios of s-processing occuring in an AGB member of a binary system). However, such an idea requires a more detailed study of a greater number of stars in order to reach a definitive conclusion. As mentioned before, HD 5223 is known to be a radial-velocity variable, and is likely a binary system. For the two HES stars our measurements are the first available accurate radial-velocity measurements, so we are unable to comment on their likely binarity.

Abundance anomalies particular to CH stars are generally explained as a result of mass transfer from a companion star that has undergone its second ascent of the giant branch, becoming an AGB star. Although such a scenario seems to explain the observed behaviour in many classical CH stars, including perhaps HE 1152−0355 and HD 5223, this cannot be generalized to the case of HE 1305+0007, which exhibits a strong double enhancement of both s-process elements (e.g., [Pb/Fe] = +2.37) and r-process elements (e.g., [Eu/Fe] = +1.97). In the following, we focus on the abundance pattern of this object for a detail discussion.

Figure 9 shows a comparison of the observed elemental abundance distribution in HE 1305+0007, relative to Ba, with the solar abundance patterns of the heavy elements associated with the r-process and s-process solar abundances, taken from Burris et al. (2000). As can be seen from inspection of this Figure, the observed n-capture abundances in HE 1305+0007 do not agree with either of the scaled r-process or s-process abundance patterns in the solar system; the general pattern is clearly non-solar. The abundance pattern labelled as "r+s" is a simple average of r-process and s-process solar abundances from Burris et al. (2000); this pattern is closer to the observed abundance pattern in HE 1305+0007 than either of the $r-$only and $s-$only patterns. While r+s indicates a simple average, it should be possible to consider a weighted average of the processes, where the weights are determined by relative fractions of r- and s-process solar abundances that could perhaps better reproduce the observed abundance pattern in HE 1305+0007.

The enhancements in Sr and Y are much lower than the enhancement in Ba, consequently the ratios [Y/Ba] and [Sr/Ba] appear particularly low. The elements with $57 \leq Z \leq 62$ have abundance distributions closer to the $r-$only curve, although La, Ce, and Pr are slightly above this curve, while Nd and Sm are slightly below it. Eu and Pb lie between the values from of the $r-$only and $s-$only solar-system curves, suggesting that the observed pattern has contributions from both the $r-$ and $s-$ processes.

The number of very metal-poor stars that are known to exhibit double enhancements of $r-$ and $s-$ process elements is still small. We consider two examples, CS 22948-027 and CS 29497-034 (Hill et al. 2000, Barbuy et al. 2005); these stars exhibit large enhancements of carbon as well as atmospheric parameters, metallicities, and heavy-element abundance patterns that are similar to HE 1305+0007. Hence, it is informative to compare the abundance pattern of HE 1305+0007 with the abundance distribution of these two stars. Radial velocity measurements show that both of the CS stars are long-period binaries (Preston & Sneden 2001, Barbuy et al. 2005), indicating that mass accretion from the (now invisible) more-massive companion occurred during its AGB phase (not RGB), explaining the observed enhancements of the s-elements, including Pb (Barbuy et al. 2005). Figure 10 shows the distribution of n-capture element abundances ([X/Fe]) versus their atomic numbers (Z) for HE 1305+0007, compared with those of CS 22948-027 and CS 29497-034. Table 7 summarizes these abundances. We notice that these three stars exhibit overabundances of the proton-capture element Na, which is believed to be formed by deep CNO-burning in massive AGB stars. In general, enhancement of the proton-capture elements Na and Al, although common in globular clusters, is not observed in field metal-poor stars. Thus, the enhancement of Na in these stars could also be an indication of pollution by an AGB companion. From the similarity in abundance distributions, these three stars seem to have originated from related nucleosynthetic and evolutionary processes. However, one should note that HE 1305+0007 has not yet been shown to be a member of a binary system.

HE 1305+0007 also exhibits a large overabundance of the 3rd peak s-process element Pb. In contrast to HE 1305+0007, all of the other known metal-poor Pb-rich stars are not rich in r-process elements. In very metal-poor AGBs, the s-process operates with a high ratio of neutrons to seed nuclei that favours production of a high abundance of Pb. According to Gallino et al. (1998), a large production of the doubly magic nucleus ^{208}Pb is due to AGB stars of low metallicity, which explains the presence of Pb in low-metallicity stars. That the low-mass AGB stars ($M \leq 4M_{\odot}$) play a dominant role in the production of $s-$elements in

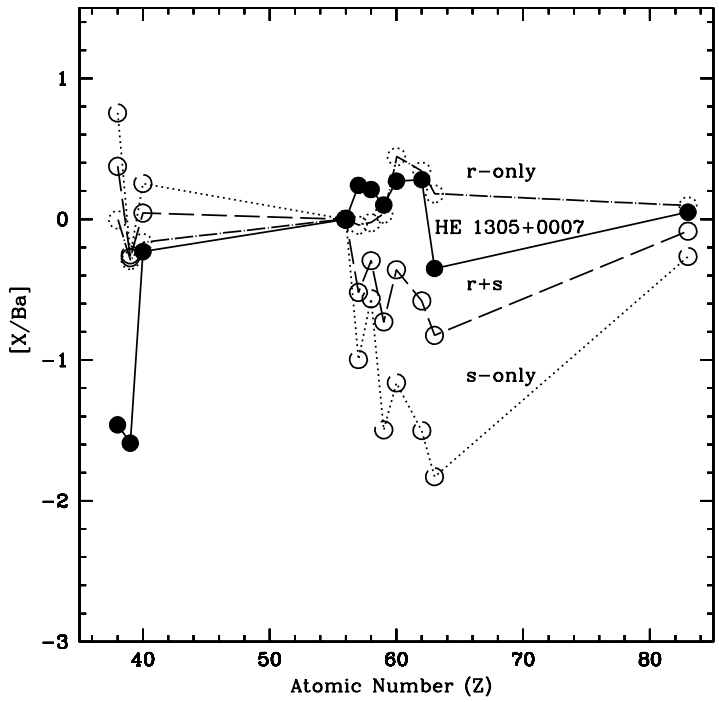

Figure 9. The patterns of the heavy elements, relative to Ba, in HE 1305+0007 are compared to the r-process and s-process solar abundances from Burris et al. (2000). The abundance pattern of HE 1305+0007 is indicated by the solid line connecting the solid circles. The dotted line indicates "s-only", the dot-dashed line indicates "r-only" and the dash line indicates and average "r+s" abundance pattern connecting the open circles.

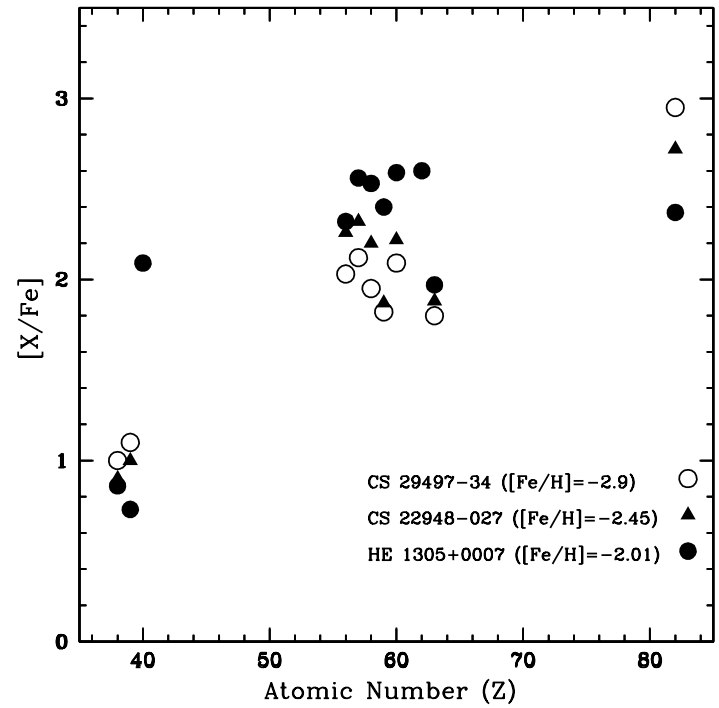

Figure 10. A comparison of the distribution of n-capture elements abundances ([X/Fe]) versus their atomic numbers (Z) in HE 1305+0007 with those of two similar objects, CS 22948-027 and CS 29497-034. The solid circles represent HE 1305+0007, the solid triangles represent CS 22948-027, and the open circles represent CS 29497-034.

Table 6: Estimation of errors. Differential abundances $\Delta\log\epsilon$ of elements with respect to those derived using the adopted model with $T_{\rm eff}$ = 4750 K, log g = 2.0, and $V_{\rm t}$ = 2.0 km s^{-1} for HE 1305+0007

Element	$\Delta T_{\rm eff}$ +250	$\Delta T_{\rm eff}$ −250	$\Delta\log g$ +0.25	$\Delta\log g$ −0.25	$\Delta V_{\rm t}$ +0.25	$\Delta V_{\rm t}$ −0.25
Na	+0.35	−0.37	−0.05	−0.04	−0.14	+0.03
Mg	+0.30	−0.50	−0.08	+0.12	−0.15	+0.05
Ca	+0.34	−0.24	+0.03	+0.06	+0.05	+0.11
Sc	+0.17	−0.15	+0.10	−0.10	−0.05	+0.04
Ti	−0.02	−0.05	+0.08	−0.10	−0.10	+0.08
Mn	+0.40	−0.55	−0.05	−0.03	−0.10	−0.06
Fe I	+0.36	−0.36	−0.02	−0.08	−0.10	+0.13
Fe II	−0.06	+0.13	+0.10	−0.17	−0.07	+0.12
Ni	+0.34	−0.28	+0.03	+0.02	+0.01	+0.05
Sr	+0.30	−0.35	+0.10	+0.04	−0.04	+0.04
Y	+0.07	−0.05	+0.10	−0.05	−0.05	+0.07
Zr	+0.40	−0.50	−0.01	+0.02	−0.01	+0.02
Ba	+0.18	−0.20	+0.04	−0.05	−0.10	+0.10
La	+0.10	−0.10	+0.08	−0.10	−0.10	+0.10
Ce	+0.10	−0.05	+0.09	−0.09	−0.10	+0.12
Pr	+0.10	−0.10	+0.08	−0.09	−0.14	+0.12
Nd	+0.05	−0.10	+0.03	−0.10	−0.10	+0.06
Sm	+0.13	−0.10	+0.10	−0.09	−0.05	+0.06
Eu	−0.05	−0.12	+0.06	−0.15	−0.12	−0.11
Pb	+0.12	−0.28	+0.03	−0.12	−0.25	−0.15

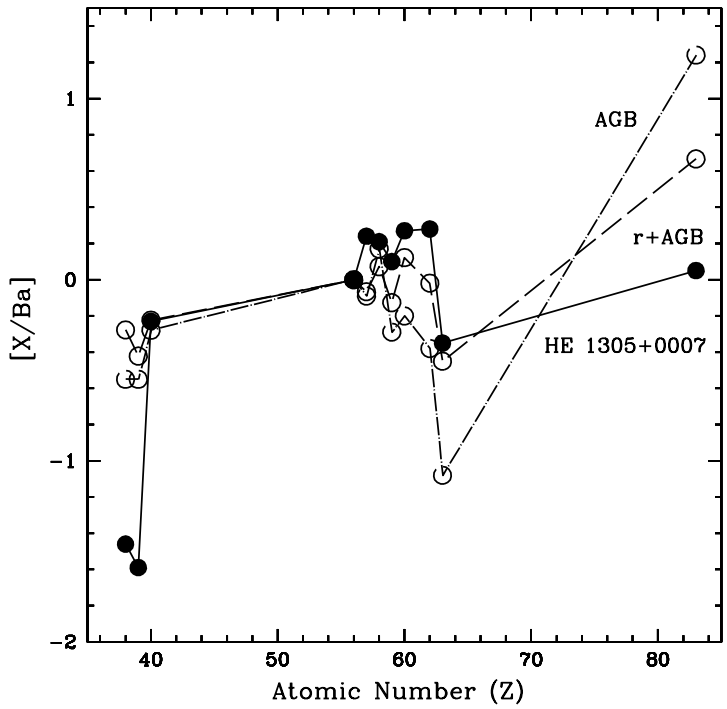

Figure 11. The patterns of the heavy elements relative to Ba in HE 1305+0007 (solid line, connecting the solid circles) are compared with the abundances predicted to be found in the dredge-up material of a low-metallicity AGB model (dot-dash line) from Goriely & Mowlavi (2000). The dashed line indicates the pattern from a simple mixture of the abundances of the low-metallicity AGB model and the solar r-process abundances.

the Galaxy was also supported by Travaglio et al. (2001). Calculations by Goriely & Mowlawi (2000) and Goriely & Siess (2001) also predict large enhancements of third-peak $s-$elements relative to the 1st and 2nd s-process peaks.

In Figure 11, we compare the abundances of HE 1305+0007 with the abundances derived from a low-mass, low-metallicity AGB model (Goriely & Mowlavi 2000). The abundance curve from the low-metallicity AGB model, scaled to match the observed Ba abundance of HE 1305+0007, does not appear to account for any of the

Table A: List of Fe lines

W_{lab}	ID	EP_{low}	loggf	HE 1305+0007 Eq widths (mÅ)	HE 1152−0355 Eq widths (mÅ)	HD 5223 Eq widths (mÅ)
6593.880	Fe I	2.4327	−2.420	—	—	68.2
6551.680	Fe I	0.9901	−5.790	—	74.7	—
6518.380	Fe I	2.8316	−2.750	—	100.8	—
6335.340	Fe I	2.1979	−2.230	—	159.9	—
6252.550	Fe I	2.4041	−1.687	86.1	—	108.2
6230.726	Fe I	2.5590	−1.281	93.8	208.0	118.4
6219.280	Fe I	2.1979	−2.430	—	206.8	—
6213.430	Fe I	2.2227	−2.660	—	186.2	—
6191.558	Fe I	2.4330	−1.600	—	195.5	117.1
6137.694	Fe I	2.5881	−1.403	101.3	—	113.9
6136.615	Fe I	2.4530	−1.400	113.2	199.2	121
6065.480	Fe I	2.6085	−1.530	—	204.8	97.75
5853.180	Fe I	1.4848	−5.280	—	67.0	—
5586.760	Fe I	3.3683	−0.210	—	—	111.8
5506.778	Fe I	0.9901	−2.797	102.8	—	—
5339.928	Fe I	3.266	−0.680	78.2	—	—
5332.899	Fe I	1.557	−2.940	72.2	—	—
5324.178	Fe I	3.211	−0.240	108.7	—	117.1
5324.179	Fe I	3.211	−0.103	—	—	117.1
5281.790	Fe I	3.0380	−1.020	74.9	—	93.0
5266.555	Fe I	2.9980	−0.492	106.6	183.5	117.8
5254.955	Fe I	0.1100	−4.764	79.9	—	105.0
5250.210	Fe I	0.1213	−4.940	—	—	85.0
5247.050	Fe I	0.0872	−4.946	—	198.1	88.4
5232.939	Fe I	2.9400	−0.190	119.2	—	134.4
5225.525	Fe I	0.1101	−4.790	—	224.3	91.6
5217.396	Fe I	3.2100	−1.097	76.2	—	—
5216.274	Fe I	1.6080	−2.150	—	—	119.5
5202.340	Fe I	2.1759	−1.838	—	208.7	103.4
5198.710	Fe I	2.2227	−2.134	—	152.1	78.5
5194.940	Fe I	1.5574	−2.090	—	228.2	—
5192.343	Fe I	2.9980	−0.521	108.4	—	108.0
5171.595	Fe I	1.4848	−1.793	133.7	—	149.9
5166.281	Fe I	0.0000	−4.190	119.6	—	—
5006.119	Fe I	2.8330	−0.610	—	—	115.3
4961.910	Fe I	3.6344	−2.280	—	54.9	—
4924.770	Fe I	2.2786	−2.222	—	156.8	—
4871.317	Fe I	2.8650	−0.410	136.9	—	—
4494.560	Fe I	2.1973	−1.140	—	—	107.3
4484.219	Fe I	3.6025	−0.720	60.0	—	73.0
4466.551	Fe I	2.8320	−0.590	122.9	—	—
5316.615	Fe II	3.1528	−1.850	94.7	—	—
5276.002	Fe II	3.1990	−1.940	76.6	—	—
5234.625	Fe II	3.2214	−2.050	61.5	78.3	80.5
4923.930	Fe II	2.8910	−1.319	—	160.3	130.2
4583.839	Fe II	2.8070	−2.020	81.8	—	110.3
4491.400	Fe II	2.8555	−2.700	—	—	55.4

stellar abundances of Sr, Y, Eu, let alone Pb. In order to check for any additional r-process contributions, the abundances of HE 1305+0007 are also compared with a simple mixture of the abundances of the low-metallicity AGB model with solar r-process abundances (scaled to match the [Ba/Eu] ratio in this star). The higher Eu abundance compared with expectation from the pure s-process models suggests some additional contribution from the r-process. However, the observed abundance pattern is clearly not adequately represented by a simple mixture of n-capture processes.

7 CONCLUSIONS

A high-resolution spectroscopic analysis of the CEMP stars HE 1305+0007 and HE 1152−0355 indicates large enhancements of C and the s-process elements relative to Fe. The 2nd-peak s-process elements are found to be more enhanced than those of the 1st-peak s-process elements. HE 1305+0007 is also found to be characterised by a large enhancement of the 3rd-peak s-process element lead ([Pb/Fe] = +2.37). The large enhancement of europium ([Eu/Fe] = +1.97) is another important feature of this star. The CEMP stars exhibiting enhancements of Pb constitutes a growing group of 29 objects; we raise this number to 30 by

Table B: Measured equivalent widths

W_{lab}	ID	EP_{low}	loggf	Eq widths (mÅ) HE 1305+0007	Eq widths (mÅ) HD 5223
4571.096	Mg I	0.0000	−5.688	140.8	138.8[as]
5172.684	Mg I	2.7117	−0.402	250.7	281.0[as]
5528.405	Mg I	4.340	−0.620	171.3	186.6[as]
6102.727	Ca I	1.880	−0.793	74.0	91.5[as]
6122.226	Ca I	1.890	−0.316	125.9	146.7[as]
5192.970	Ti I	0.0211	−0.950	138.9	—
4534.780	Ti I	0.8360	0.336	119.4	131.0[as]
4805.090	Ti II	2.0613	−1.100	98.7	112.5[as]
4798.507	Ti II	1.0800	−2.670	84.4	96.4[as]
5432.546	Mn I	0.0000	−3.795	31.4	—
5420.370	Mn I	2.1427	−1.460	43.0	—
6314.653	Ni I	1.9355	−1.770	45.8	59.3[as]
6111.060	Ni I	4.0882	−0.870	81.2	57.5[as]
4937.340	Ni I	3.6060	−0.390	124.5	162.6
4607.327	Sr I	0.000	−0.570	64.0	70.3
5200.406	Y II	0.9923	−0.570	74.2	90.2[as]
5205.731	Y II	1.0330	−0.342	93.0	103.9[as]
6134.570	Zr I	0.0000	−1.280	30.1	19.7[as]
6496.897	Ba II	0.6040	−0.369	379.0	343.1[as]
6141.727	Ba II	0.704	−0.069	390.0	300.4
5853.668	Ba II	0.6040	−1.020	243.7	211.7[as]
5188.206	La II	2.4488	−0.010	49.6	43.48[as]
5259.380	La II	0.1729	−1.760	97.7	85.37[as]
4773.941	Ce II	0.9243	−0.498	76.6	71.99
5512.062	Ce II	1.0082	−0.518	93.0	84.8[as]
5274.229	Ce II	1.0444	−0.323	103.0	100.7[as]
5259.728	Pr II	0.6334	0.080	110.6	96.4[as]
5825.851	Nd II	1.0807	−0.760	76.9	48.3
5718.120	Nd II	1.4100	−0.510	80.0	63.1
5688.530	Nd II	0.9860	−0.250	90.2	75.1
5319.820	Nd II	0.550	−0.210	133.3	114.8
5293.169	Nd II	0.8230	−0.060	121.9	106.7[as]
5287.133	Nd II	0.7446	−1.300	60.2	38.5
5276.869	Nd II	0.8590	−0.610	86.4	64.3[as]
5255.506	Nd II	0.2046	−0.820	126.5	114.4
5249.590	Nd II	0.9760	0.210	114.8	96.5
5212.361	Nd II	0.2046	−0.870	115.9	99.85[as]
4859.039	Nd II	0.3200	−0.830	104.7	102.0
4791.597	Sm II	0.1000	−1.846	65.2	42.4
4615.456	Sm II	0.5400	−1.262	83.0	67.8[as]

"as" indicates lines are asymmetric

adding HE 1305+0007. In addition, this star is likely to be one of a small number that exhibit double enhancement of r-process and s-process elements, the CEMP-r/s group. The large enhancements of n-capture elements exhibited by the classical CH star HD 5223 is consistent with the abundance pattern generally noticed in other CH stars. The enhancement of s-process elements in this star, along with the large enhancement of carbon, indicate that a mass-transfer event in a binary system from a companion AGB star that underwent s-process nucleosynthesis during its lifetime. However, in HE 1305+0007, the enhanced Eu abundance, together with the large abundance of the 3rd-peak s-process element Pb, presents a challenge to understanding the formation mechanism of this star. Among several scenarios proposed, the possibility that a star with a high ratio of r-elements/Fe could, by accreting some s-rich matter, become an r/s star with a large [Eu/Fe], has been discussed by many authors. A scenario invoking a triple system, one component polluting the presently-observed star with r-elements, and another polluting with s-elements has also been considered in the literature, but was discarded on the grounds that such a triple system may not be dynamically stable (Cohen et al. 2003). Qian & Wasserburg (2003) suggested that the double enhancement in the CEMP-r/s stars could be due to the s-process occurring in an AGB member of a binary system, followed by the r-process taking place in a subsequent accretion induced collapse (AIC) of the white dwarf remnant of the former AGB. However, the expected rate of the occurence of AIC events in the Galaxy is low and highly uncertain. This rarity cannot justify the substantial fraction of CEMP-r/s stars ($\sim 30\%$) observed among all the CEMP$-s$ stars (Bailyn & Grindlay 1990, Qian & Wasserburg 2003).

Zijlstra (2004) proposed a different scenario, in which the primary (evolved to an AGB star) transfers s-rich matter to the observed star, but does not suffer large mass loss (owing to its low metallicity). At the end of the AGB phase,

Table 7: Abundances of HE 1305+0007 compared with CS 22948-027 and CS 29497-034

Elements X	Z	$\log \epsilon$ Solar	[X/Fe] HE 1305+0007 [Fe/H] = −2.0 [hs/ls] = 1.22 $^{12}C/^{13}C = 10$	[X/Fe] CS 22948-027 [Fe/H] = −2.45 [hs/ls] = 0.97 $^{12}C/^{13}C = 14$	[X/Fe] CS 29497-034 [Fe/H] = −2.9 [hs/ls] = 1.28 $^{12}C/^{13}C= 12$
C I	6	8.39	+1.84	+2.43	+2.63
Na I	11	6.17	+0.26 (D_2)	+0.57	+1.18
Na I	11	6.17	+0.43 (D_1)	+0.57	+1.18
Ca I	20	6.31	+0.13	+0.54	+0.45
Sc II	21	3.05	+0.09	—	—
Ti I	22	4.90	—	+0.34	+0.29
Ti II	22	4.90	+0.79	+0.54	+0.44
Mn I	25	5.39	+0.14	—	—
Ni I	28	6.23	−0.25	−0.01	+0.01
Sr I	38	2.92	+0.86	—	—
Sr II	38	2.92	—	+0.90	+1.00
Y II	39	2.21	+0.73	+1.00	+1.10
Zr I	40	2.59	+2.09	—	—
Ba II	56	2.17	+2.32	+2.26	+2.03
La II	57	1.13	+2.56	+2.32	+2.12
Ce II	58	1.58	+2.53	+2.20	+1.95
Pr II	59	0.71	+2.38	+1.65	+1.65
Nd II	60	1.45	+2.59	+2.22	+2.09
Sm II	62	1.01	+2.60	+1.70	+2.00
Eu II	63	0.52	+1.97	+2.10	+2.25
Pb I	82	2.00	+2.37	+2.72	+2.95

the degenerate core explodes as an AGB supernova. However, r-processing in such a scenario is not expected to be significant.

A formation scenario for these stars involving high-mass AGB stars (8-10 $M_\odot$) was discussed at length by several authors (e.g., Barbuy et al. 2005, Wanajo et al. 2006). The possibility of s-processing occurring in a 10 solar mass star with an O-Ne-Mg core has been studied by Ritossa et al. (1996); these authors demonstrated that the reaction $^{22}Ne(\alpha, n)^{25}Mg$ is efficient in such high-mass stars, owing to the high temperature 3×10^8 K reached at the base of the He-convective shell. An astrophysical scenario associated with the AGB star in a binary system, in which the r-process might also occur, appears to be a positive step toward understanding the formation mechanisms of the CEMP-r/s stars. More quantitative studies of s-process nucleosynthesis in this mass range is needed in order to make definitive conclusions. A detailed and comprehensive discussion on several of the proposed formation scenarios of CEMP-r/s stars is provided by Jonsell et al. (2006).

While in the present work we discuss the carbon and neutron-capture element abundance distribution for only three CEMP stars, we intend to conduct additional analyses for a larger sample of stars in the near future. Aoki et al. (2006) provides one such study, including over 20 CEMP stars. Cohen et al. (2006) describes a sample of 16 CEMP stars. An analysis of the abundance patterns obtained from consideration of larger samples will permit one to put the role of CEMP stars in the early history of Galactic chemical evolution into better perspective. It is also important to seek measurements of the crucial species Li, O, Na, and the mixing diagnostic $^{12}C/^{13}C$ ratio for these expanded samples of CEMP stars. In addition to many theoretical propositions (Gallino et al. 1998, Goriely & Mowlavi 2000, Goriely & Siess 2001), there now exists observational evidence that suggests, in contrast to the $r-$only hypothesis of Truran (1981), that the s-process could indeed operate even at very low metallicities, as low as [Fe/H] = −3.1 (Johnson & Bolte 2002). Sivarani et al. (2006) report on three unevolved (main-sequence turnoff) CEMP stars, at least one of which (CS 29528-041) exhibits moderately high [Ba/Fe] ($\sim$ +1.0) at a metallicity [Fe/H] = −3.3. Masseron et al. (2006) describe the remarkable discovery of an apparent thermally-pulsing AGB star, CS 30322-023, which exhibits a clear s-process signature, at [Fe/H] = −3.5. Obviously, there are many surprises yet to be revealed concerning the operation of the s-process in the early Galaxy. Although uncertain, it also seems likely that the impact of an early s-process on the chemical evolution of carbon, nitrogen, oxygen, and the neutron-capture elements in the Galaxy will critically depend on the Initial Mass Function of early-generation stars (Abia et al. 2001; Lucatello et al. 2005; Karlsson 2006).

Acknowledgements

This work made use of the SIMBAD astronomical database, operated at CDS, Strasbourg, France, and the NASA ADS, USA.

T.C.B. acknowledges partial funding for this work from grant AST 04-06784, as well as from grant PHY 02-16783: Physics Frontiers Center/Joint Institute for Nuclear Astrophysics (JINA), both awarded by the U.S. National Science Foundation. N.C. acknowledges financial support by Deutche Forschungsgemeinschaft through grants Ch 214/3 and Re 353/44. He is a research fellow of the Royal Swedish Academy of Sciences supported by a grant from the Knut and Alice Wallenberg Foundation. J.E.N. acknowledges sup-

port from Australian Research Council grant DP0342613.

REFERENCES

Abia, C., Dominguez, I., Staniero, O. et al., 2001, ApJ, 557, 126
Alonso A., Arribas S. & Martinez-Roger C., 1994 A&AS, 107, 365
Alonso A., Arribas S. & Martinez-Roger C., 1996 A&A, 313, 873
Alonso A., Arribas S. & Martinez-Roger C., 1998 A&AS, 131, 209
Aoki W. & Tsuji T., 1997, A&A, 317, 845
Aoki W., Ryan S. G., Norris J. E., Beers T. C., Ando H., & Tsangarides S., 2002, ApJ, 580, 1149
Aoki, W., Beers, T.C., Christlieb, N., Norris, J.E., Ryan, S.G., & Tsangarides, S. 2006, ApJ (submitted)
Arribas S. & Martinez-Roger C., 1987, A&AS, 70, 303
Asplund M., Grevesse N. & Sauval A. J., 2005, ASPC, 336, 25
Bailyn C. D. & Grindlay J. E., 1990, ApJ, 353
Barbuy B., Spite M., Spite F., Hill V., Cayrel R., Plez B., Petitjean P., 2005, A&A, 429, 1031
Baumüller D., Butler K., & Gehren T., 1998, A&A, 338, 637
Baumüller D. & Gehren, T., 1997, A&A, 325, 1088
Beers T. C., 1999, ASPC, 165, 202
Beers T. C. & Christlieb N., 2005, ARAA, 43, 561
Beers T. C., Preston G. W., Shectman S. A., 1992, AJ, 103, 1987
Beers T. C., Flynn C., Rossi S., Christlieb N., Sommer-Larsen J., et al. 2006, ApJS (submitted)
Bonifacio P., Molaro P., Beers T. C., Vladilo G., 1998, A&A, 332, 672
Burris D. L., Pilachowski C. A., Armandroff T. E., Sneden C., Cowan John J., Roe H., 2000, ApJ, 544, 302
Burstein D., Heiles, C., 1982, AJ, 87, 1165
Busso M., Gallino R., & Wasserburg G. J., 1999, ARA&A, 37, 239
Carney Bruce W., Latham David W., Laird, John B., Aguilar, Luis A., 1994, AJ, 107, 2240
Cayrel R., Depagne E., Spite M., Hill V., et al. 2004, A&A, 416, 1117
Christlieb N., 2003, RvMA, 16, 191
Christlieb N., Green P. J., Wisotzki L., Reimers D., 2001, A&A, 375, 366
Cohen J. G., Christlieb N., Qian Y.-Z., Wasserburg G. J., 2003, ApJ, 588, 1082
Cohen J.G., McWilliam A., Shectman S., Thompson I., Christlieb N., Melendez J., Ramirez S., Swensson A., & Zickgraf F.-J., 2006, AJ, in press (astro-ph/0603582)
Cutri R.M., Skrutskie M. F., Van Dyk S., et al. 2003, Explanatory Supplement to the 2MASS All Sky Data Release, http://www.ipac.caltech.edu/2mass/releases/allsky/doc/explsup.html
Fuhr J. R., Martin G. A. & Wiese W. L., 1988, J. Phys. Chem. Ref. Data, 17, No 4
Gallino R., Arlandini C., Busso M. et al., 1998, ApJ, 497, 388
Goriely S. & Mowlavi N., 2000, A&A, 362, 599
Goriely S., & Siess N., 2001, A&A, 378, L25
Goswami A. 2005, MNRAS, 359, 531
Goswami A. & Prantzos N., 2000, A&A, 359, 191
Green P. J., Margon B., Anderson Scoff F., Cook K. H., 1994, ApJ, 433, 319
Hill V., Barbuy B., Spite M., et al., 2000, A&A, 353, 557
Iben I. & Renzini A., 1982, ApJ, 263, L23
Johnson JA. & Bolte M., 2002, ApJL, 579, L87-90
Jonsell K., Barklem P.S., Gustafsson B., Christlieb N. et al., 2006, A&A,in press (astro-ph/0601476)
Karlsson T., 2006, ApJL, 641, L41
Lambert D. L., Heath J. E., Lemke M., Drake J., 1996, ApJS, 103, 183
Lawler J. E., Bonvallet G. & Sneden C., 2001, ApJ, 556, 452
Lucatello S., Gratton R. G., Beers T. C., Carretta E., 2005, ApJ 625, L833-837
Masseron T., Van Eck S., Famaey B., Goriely S., Plez B., Siess L., Beers T.C., Primas F., & Jorissen A., 2006, A&A, in press
McClure R. D., Woodsworth W., 1990, ApJ, 352, 709
Martin G. A., Fuhr J. R. & Wiess, W. L., 1988, J. Phys. Chem. Ref. data, 17, No 3
McWilliam A., Preston G. W., Sneden C., & Searle L., 1995, AJ, 109, 27
Noguchi K., Aoki W., Kawanomoto S., Ando H. et al., 2002, PASJ, 54, 855
Norris J. E., Ryan S. G., Beers T. C., 1997a, ApJ, 488, 350
Norris J. E., Ryan S. G., Beers T. C., 1997b, ApJ, 489, L169
Norris, J. E., Ryan, S. G., Beers, T. C., Aoki, W. & Ando, H., 2002, ApJ, 569, L107
Preston G. W. & Sneden C., 2001, AJ, 122, 1545
Qian Y.-Z, & Wasserburg G. J., 2003, ApJ, 588, 1099
Ritossa C., Garcia-Berro Enrique, Iben Icko Jr., 1996, ApJ, 460, 489
Ryan S. G., Norris J. E., Beers T. C., 1996, ApJ, 471, 254
Schlegel D. J., Finkbeiner D. P., Davis M., 1998, ApJ, 500, 525
Sivarani T., Beers T.C., Bonifacio P., Molaro P., Cayrel R., Herwig, F., Spite M., Spite F., Plez Andersen J., Barbuy B., Depagne E., Hill V., Francois P., Nordström, B., & Primas F., 2006, A&A, (submitted)
Skrutskie M. F., Cutri R. M., Stiening R., Weinberg, M. D. et al., 2006, 2006, AJ, 131, 1163
Sleivyte J. & Bartkevicius A., 1990, Vilinius Astron. Obs. Bull.85, 3
Sneden C., 1973, PhD thesis, Univ of Texas at Austin
Sneden C., McWilliam A., Preston G. W., Cowan, John J., Burris, D. L., Armosky B. J., 1996, ApJ, 467, 819
Totten E. J. & Irwin M. J., 1998, MNRAS, 294, 1
Travaglio C., Gallino R., Busso M. & Gratton R., 2001, ApJ, 549, 346
Truran J. W., 1981, A& A, 97, 391
Tsuji T., Tomioka K., Sato H., Iye M., Okada T., 1991, A&A, 252, L1
Vanture, A. D., 1992, AJ, 104, 1997
Wanajo S., Nomoto K., Iwamoto N., Ishimaru Y., & Beers T. C., 2006, ApJ, 636, 842
Zijlstra A. A., 2004, MNRAS, 348, L23